SCIENCE CHINA
Information Sciences

• RESEARCH PAPER •

August 2016, Vol. 59 082201:1–082201:16
doi: 10.1007/s11432-015-0763-9

CW interference mitigation in GNSS receiver based on frequency-locked loop

Hongyu REN, Yongqing WANG*, Lei JIANG & Siliang WU

School of Information and Electronics, Beijing Institute of Technology, Beijing 100081*, China*

Received March 13, 2016; accepted April 8, 2016; published online June 16, 2016

Abstract Global navigation satellite system (GNSS) receivers are highly susceptible to continuous wave (CW) interference because the received signals are extremely weak. Current interference mitigation techniques mainly use a notch filter or transform domain. This paper proposes a computationally effective algorithm based on a frequency-locked loop (FLL) to mitigate interference in GNSS receivers. The performance of the algorithm is validated through an analysis of the characteristics of the interference reduction filter and interference estimation precision. A Monte Carlo simulation is used to compare the proposed algorithm with various previous algorithms: the adaptive IIR notch filter, adaptive linear-phase FIR filter, and N-sigma DFT algorithm. The simulation results show that the proposed algorithm exhibits excellent interference estimation precision and superior anti-jamming performance compared with the conventional algorithms.

Keywords continuous wave mitigation, frequency-locked loop, interference reduction filter, interference estimation, code tracking

Citation Ren H Y, Wang Y Q, Jiang L, et al. CW interference mitigation in GNSS receiver based on frequency-locked loop. Sci China Inf Sci, 2016, 59(8): 082201, doi: 10.1007/s11432-015-0763-9

1 Introduction

A global navigation satellite system (GNSS) receiver inherently has anti-interference ability because of its spread spectrum characteristics. Nevertheless, GNSS signals are very weak and can be easily corrupted by intentional or unintentional interferences, leading to significant degradation in GNSS tracking and positioning performance [1]. Continuous wave (CW) interference is one of the most insidious interference sources that cause severe performance degradation in the GNSS receiver [2–4].

CW interference reduction techniques have attracted considerable attention recently [5, 6] and can be classified into time- and frequency-domain approaches. Among the time-domain algorithms, the most frequently employed interference mitigation scheme is based on adaptive notch filters [7–9]. Borio et al. [10] proposed a detection scheme for CW interference based on an adaptive infinite impulse response (IIR) notch filter that adaptively estimates the notch frequency. IIR is the most widely employed class of notch filter structures because of its low computational complexity and efficient implementation. However, the IIR notch filter degrades the quality of useful signals to a large extent and introduces time delays [11]. Abdizadeh et al. [8] used a linear-phase finite impulse response (LP-FIR) notch filter to efficiently detect

* Corresponding author (email: wangyongqing@bit.edu.cn)

and track CW interference and properly eliminate it without causing phase distortion. Although FIR filters can be easily designed to have a linear phase frequency response, linear phase FIR notch filters have a higher computational load than IIR ones. Moreover, the matrix of its adaptive process is too complicated to be implemented on hardware. The use of a frequency-domain interference suppressor is also a popular interference mitigation technique; it is frequently mentioned in the literature and is commonly used in working receivers [12]. Capozza et al. [13] employed a discrete Fourier transform (DFT) algorithm to detect and remove abnormal spectral lines from the received signal's band. Balaei and Dempster [14] devised a statistical hypothesis to detect GPS interference in the frequency domain. Other currently used efficient approaches include interference mitigation filters in the transform domain, such as the short-time Fourier transform (STFT) [5] and the wavelet transform (WT). However, the biggest concern associated with the abovementioned transform domain approaches is hardware complexity. Moreover, mitigation performance is limited by significant spectral leakage.

Therefore, in this paper, a CW interference mitigation algorithm based on a frequency-locked loop (FLL) is proposed. This method is based on the time domain, but is not limited to the notch filter and its corresponding adaptive algorithm. In the proposed algorithm, the single sinusoidal interference is converted to a direct current (DC) signal through spectrum shifting, and is eliminated by subtracting the DC component. The estimation of the DC component can be realized by an integrator, while the spectrum shifting process can be implemented by the correlator of an FLL or a phase-locked loop (PLL). Both the FLL and PLL have perfect interference tracking performance, and because the dynamic adaptation ability of the FLL is considerably better, we use the FLL. Therefore, the notch filter and adaptive module in the traditional algorithms are replaced by the mitigation integrator and FLL in the proposed algorithm. Naturally, the filter characteristics of the mitigation integrator and the interference tracking precision of the FLL determine the interference suppression performance of this method. Various aspects of the proposed algorithm are analyzed. A comparison with previously reported mitigation methods is performed and appropriate metrics in [5] are introduced to validate the effectiveness of the proposed algorithm.

This paper defines an algorithm for interference mitigation that is to be implemented in GNSS receivers for high-precision navigation. Conventional time- and frequency-domain approaches cannot meet the requirements for application because of their respective defects. The difference between the FLL-based method and frequency-domain methods is that the proposed algorithm addresses the spectral leakage problem and avoids the complex time-frequency transform. The difference between the FLL-based method and LP-FIR notch filter methods is that the proposed algorithm provides stronger interference mitigation with less resource consumption. The difference between the FLL-based method and IIR notch filter methods is that the proposed algorithm has better phase characteristics, which is useful for positioning accuracy. The excellent interference estimation precision is demonstrated in the FLL-based method. Thus, the interference can be effectively filtered out with negligible side effects on the desired signal through a simple calculation process. The proposed method is a good candidate because it implements a number of options for CW interference mitigation.

The remainder of this paper is organized as follows. Section 2 describes the GNSS signal model in the presence of CW interference. In Section 3, the design of the single interference mitigation algorithm is introduced and explained. A cascaded interference mitigation unit design is introduced for multiple interferences. Section 4 details the performance analysis of the interference mitigation algorithm. In Section 5, the Monte Carlo simulation results validate the theoretical analysis and the effectiveness of the proposed algorithm. Finally, conclusion is presented in Section 6.

2 Signal model

According to [1], the signal obtained by the output of a GNSS front-end is expressed as

$$r[n] = s[n - \tau_0] + j[n] + \eta[n], \tag{1}$$

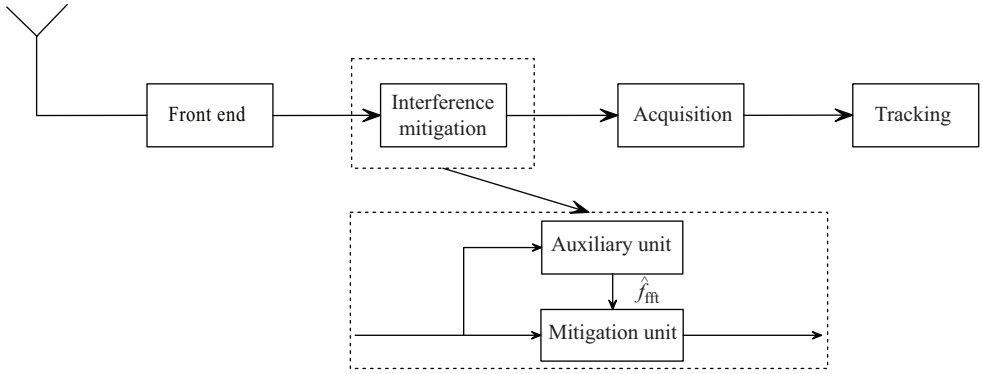

Figure 1 Operational scheme of the proposed algorithm.

where $s[n-\tau_0]$ is the received GNSS signal, τ_0 is the delay of the incoming signal, $j[n]$ is the CW interference, and $\eta[n]$ is the additive white Gaussian noise (AWGN) with zero mean and two-sided power spectral density of $N_0/2$. The GNSS signal can be modeled as

$$s[n-\tau_0] = Ac[n-\tau_0]\,d[n-\tau_0]\,\mathrm{e}^{\mathrm{i}[2\pi(f_0+f_d)n+\theta]}, \tag{2}$$

where A is the amplitude of $s[n]$, $c[n]$ is pseudo random noise code (PRN) sequence, $d[n]$ represents the navigation message, and f_0, f_d, and θ denote the intermediate frequency, Doppler frequency, and initial carrier phase of the incoming signal, respectively. The interference signals are assumed to be multitone CW interferences and can be expressed as

$$j[n] = \sum_{i=1}^{M} A_i \mathrm{e}^{\mathrm{i}(2\pi f_i n+\theta_i)}, \tag{3}$$

where M is the number of continuous waves entering the GNSS front-end bandwidth, and A_i, f_i, and θ_i denote the amplitude, frequency, and phase of the i-th sinusoid interference, respectively. The quality of the signal recovered by the front-end is indicated by means of the interference-to-noise ratio given as

$$\mathrm{JNR} = \frac{{A_i}^2}{2N_0B_f}, \tag{4}$$

where B_f is the one-sided bandwidth of the GNSS front-end. This quantity measures the relative power of the interfering signal with respect to the noise.

3 Algorithm design

3.1 Single CW interference

In this section, we propose an FLL-based CW interference mitigation algorithm implemented between the front end and acquisition stages. The general scheme of the proposed algorithm in a GNSS receiver is illustrated in Figure 1. The design of the interference mitigation algorithm includes two parts: the mitigation unit (MU) and the auxiliary unit (AU). The MU adopts FLL to track and suppress interference, whereas the AU based on DFT is used for providing a rough estimation of the interference frequency that assists the FLL in tracking the interference.

3.1.1 *Mitigation unit*

The MU mainly completes the accurate tracking and removal of the interference. An MU based on FLL shown in Figure 2 was used in this study. The MU includes two processes: FLL and interference mitigation.

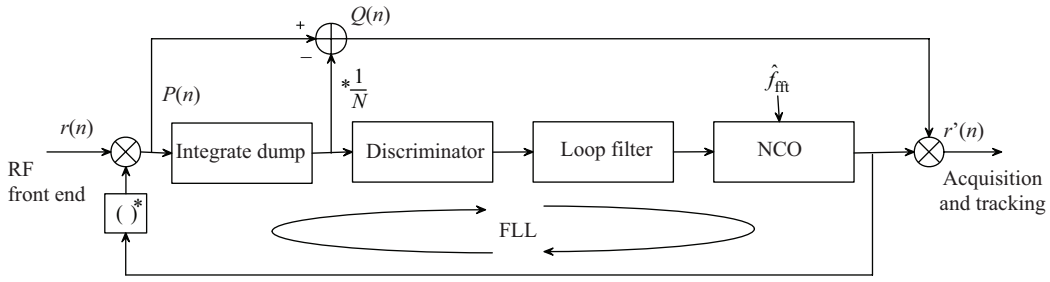

Figure 2 Block diagram of the mitigation unit design.

The FLL process tracks the interference by estimating the frequency error between the received and local signals. As in any other classical feedback control loop, the frequency difference estimated from the discriminator is filtered by a low-pass loop filter and then used to control a numerically controlled oscillator (NCO) [15, 16]. Here, it is assumed that a DFT rough estimate of the interference frequency has been given to the NCO module by the AU to extend the frequency discrimination range of the FLL. Therefore, the FLL tracks the interference depending on the difference between the interference frequency f_i and estimated interference frequency $\hat{f}_i$, where $\hat{f}_i = \hat{f}_{\text{fft}} + \hat{f}_{\text{fll}}$, and $\hat{f}_{\text{fft}}$ and $\hat{f}_{\text{fll}}$ are the rough and accurate estimates of the interference frequency provided by the DFT and FLL, respectively.

The mitigation process can be divided into three steps. The first step is down-converting. When the frequency of the reference signal generated by the NCO is aligned with the interference frequency, the interference complex signal $j\,[n]$ is down-converted around zero frequency through the correlation process. Therefore, the interference in the received signal is transformed to an approximate DC voltage signal. The down-conversion process is completed by the conjugated NCO signal. In the implementation, the in-phase component of the NCO signal remains unchanged, and the quadrature component of the NCO signal is negated. The down-converted signal can be derived as

$$\begin{aligned} P\,[n] &= r\,[n] \times \exp\left\{-\mathrm{i}\left[2\pi\hat{f}_i n + \hat{\theta}_i\right]\right\} \\ &= s\,[n-\tau_0]\,\mathrm{e}^{-\mathrm{i}\left(2\pi\hat{f}_i n+\hat{\theta}_i\right)} + A_i\mathrm{e}^{\mathrm{i}(2\pi f_e n+\theta_e)} + \eta\,[n]\,\mathrm{e}^{-\mathrm{i}\left(2\pi\hat{f}_i n+\hat{\theta}_i\right)}, \end{aligned} \tag{5}$$

where $f_e = f_i - \hat{f}_i$, $\theta_e = \theta_i - \hat{\theta}_i$.

Next, the interference signal is expected to be removed after the correlation process. The interference is mitigated by eliminating the DC component in the down-converted signal. The DC component of the down-converted signal is expressed as a mean of the signal in a certain period of time. In particular, this period can be set as the integrate-dump time T. The output of the integrate-dump component at the k-th loop update time epoch can be written as

$$\begin{aligned} \sum_{n=1}^{N} P\,[n] &= \sum_{n=1}^{N}\left\{s\,[n-\tau_0]\,\mathrm{e}^{-\mathrm{i}\left(2\pi\hat{f}_i n+\hat{\theta}_i\right)} + A_i\mathrm{e}^{\mathrm{i}(2\pi f_e n+\theta_e)} + \eta\,[n]\,\mathrm{e}^{-\mathrm{i}\left(2\pi\hat{f}_i n+\hat{\theta}_i\right)}\right\} \\ &= \left[\sum_{n=1}^{N}\left\{s\,[n-\tau_0]\,\mathrm{e}^{-\mathrm{i}\left(2\pi\hat{f}_i n+\hat{\theta}_i\right)}\right\} + \sum_{n=1}^{N}\left\{\eta[n]^{-\mathrm{i}\left(2\pi\hat{f}_i n+\hat{\theta}_i\right)}\right\}\right. \\ &\quad \left. + NA_i\mathrm{sinc}\,(\pi f_e T)\,\mathrm{e}^{\mathrm{i}\left[2\pi f_e\left(t_k+\frac{T}{2}\right)+\theta_e\right]}\right], \end{aligned} \tag{6}$$

where $N = Tf_s$ is the sampling number within the integration time. Next, we eliminate the CW interference by subtracting the mean of integrate-dump result. The treated down-converted signal can be derived as

$$\begin{aligned} Q\,[n] &= P\,[n] - \frac{1}{N}\sum_{n=1}^{N} P\,[n] \\ &= s\,[n-\tau_0]\,\mathrm{e}^{-\mathrm{i}\left(2\pi\hat{f}_i n+\hat{\theta}_i\right)} + \eta\,[n]\,\mathrm{e}^{-\mathrm{i}\left(2\pi\hat{f}_i n+\hat{\theta}_i\right)} \end{aligned}$$

$$+\left\{A_i\mathrm{e}^{\mathrm{i}(2\pi f_e n+\theta_e)}-A_i\mathrm{sinc}\left(\pi f_e T\right)\mathrm{e}^{\mathrm{i}\left[2\pi f_e\left(t_k+\frac{T}{2}\right)+\theta_e\right]}\right\}$$
$$-\frac{1}{N}\sum_{n=1}^{N}s\left[n-\tau_0\right]\mathrm{e}^{-\mathrm{i}\left(2\pi\hat{f}_i n+\hat{\theta}_i\right)}-\frac{1}{N}\sum_{n=1}^{N}\eta\left[n\right]\mathrm{e}^{-\mathrm{i}\left(2\pi\hat{f}_i n+\hat{\theta}_i\right)}. \tag{7}$$

Note that when FLL tracks the interference in stable conditions, $f_e\approx 0$; thus, we have

$$A_i\mathrm{e}^{\mathrm{i}(2\pi f_e n+\theta_e)}-A_i\mathrm{sinc}\left(\pi f_e T\right)\mathrm{e}^{\mathrm{i}\left[2\pi f_e\left(t_k+\frac{T}{2}\right)+\theta_e\right]}\approx 0. \tag{8}$$

This implies that the interference component is removed. In the implementation of this step, the in-phase signal and the quadrature signal subtract their mean value. Here, there is no need to track the phase of the interference. This is one of the reasons for using the FLL rather than the PLL. Besides, in (7), when N is sufficiently large, the mean of the noise and the down-converted spreading spectrum signal is almost zero.

$$\frac{1}{N}\sum_{n=1}^{N}s\left[n-\tau_0\right]\mathrm{e}^{-\mathrm{i}\left(2\pi\hat{f}_i n+\hat{\theta}_i\right)}\approx 0, \tag{9}$$

$$\frac{1}{N}\sum_{n=1}^{N}\eta\left[n\right]\mathrm{e}^{-\mathrm{i}\left(2\pi\hat{f}_i n+\hat{\theta}_i\right)}\approx 0. \tag{10}$$

Hence, the treated down-converted signal becomes

$$Q\left[n\right]\approx s\left[n-\tau_0\right]\mathrm{e}^{-\mathrm{i}\left(2\pi\hat{f}_i n+\hat{\theta}_i\right)}+\eta\left[n\right]\mathrm{e}^{-\mathrm{i}\left(2\pi\hat{f}_i n+\hat{\theta}_i\right)}. \tag{11}$$

Finally, the useful component in the down-converted signal should be restored by up-converting. For up-converting, the down-converted signal is correlated with the NCO signal again. After the second correlation process, the restored signal is obtained as

$$\begin{aligned} r'\left[n\right]&=Q\left[n\right]\times\exp\left\{\mathrm{i}\left[2\pi\hat{f}_i n+\hat{\theta}_i\right]\right\}\\ &\approx s\left[n-\tau_0\right]+\eta\left[n\right]. \end{aligned} \tag{12}$$

Consequently, the interference component in the received signal is filtered out and the useful signal is completely restored.

In order to explain the interference suppression process in the proposed algorithm, an example is given with the signal spectrum depicted in Figure 3. The interference has a frequency deviation of 162 kHz relative to the intermediate frequency. The signal source is noise free for better highlighting the interference removal process. Figure 3(a) shows the frequency spectrum of the received signal $r\left[n\right]$. Note that the useful signal is overpowered by interference. After being multiplied by the conjugated NCO signal, the received signal is spectrum shifted, as shown in Figure 3(b). Then, the interference component is suppressed; the signal spectrum is demonstrated in Figure 3(c). It can be clearly observed that a pseudocode signal spectrum emerges when the interference is removed. Finally, the spectrum of the restored signal is shown in Figure 3(d). Note that the useful signal remains intact, and is identical with the spectrum of the spread spectrum signal $s\left[n\right]$.

During implementation, because the integral time N could not be infinite and the filter performance of the mitigation integrator was not ideal, the terms in (10) could not be exactly equal to zero, thereby generating the interference estimation error. In the proposed algorithm, the interference is estimated as the difference between the input signal $r\left[n\right]$ and the output signal $r'\left[n\right]$:

$$\hat{j}\left[n\right]=r\left[n\right]-r'\left[n\right]. \tag{13}$$

The interference estimation error can be expressed as

$$e\left[n\right]=j\left[n\right]-\hat{j}\left[n\right]. \tag{14}$$

The interference estimation performance of the proposed algorithm will be analyzed in detail in Section 4.

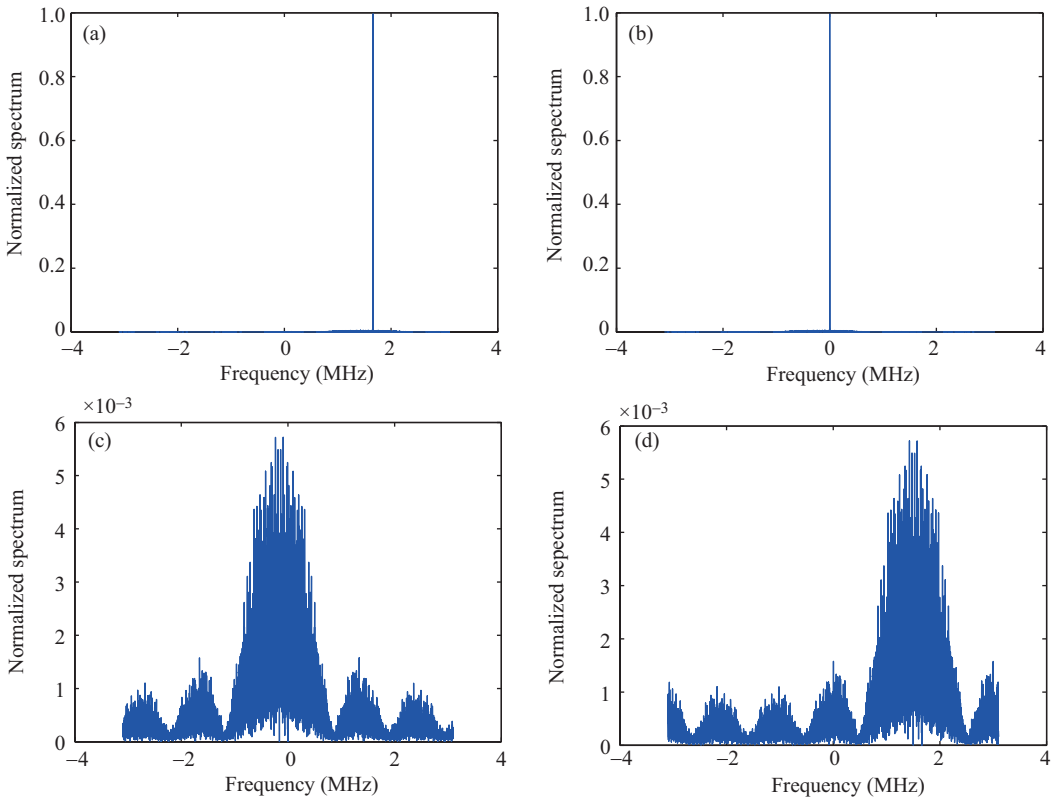

Figure 3 (Color online) Signal spectrum of the interference suppression process. (a) Received signal; (b) down-converted signal; (c) treated down-converted signal; (d) restored signal.

3.1.2 *Auxiliary unit*

The FLL has a wide frequency tracking range. Nevertheless, the interference frequency may be located at arbitrary frequency points within the full band range that the FLL cannot track. Hence, a simple DFT unit is adopted for assisting the MU.

For the DFT unit, rough interference frequency estimation should be provided. As the DFT unit in the proposed algorithm does not directly eliminate interference, it lowers the accuracy requirements. The existing residual frequency error will be gradually removed by FLL tracking. Besides, a number of developed DFT technologies such as interpolation using Fourier coefficients can be applied to the estimation of the interference frequency. The techniques employed for detecting and identifying single or multiple CW signals can be referenced in the literature [17, 18].

The design requirements of the AU are provided below. The discrimination range of the FLL depends on the selected frequency discriminator. A four-quadrant arctangent (Atan2) discriminator is one of the best discriminators because of the rarity of the data bit sign transitions modulated on the interference [16]. For the four-quadrant arctangent discriminator, the discrimination range can be expressed as

$$F_{\text{discrim}} = \left[\frac{-1}{2T}, \frac{+1}{2T}\right]. \tag{15}$$

Hence, in order to assist the FLL, the frequency estimation error of the designed DFT should not exceed the frequency discrimination range of the FLL; thus, it elicits the accuracy requirements for the AU.

$$\left|\hat{f}_{\text{fft}} - f_i\right| < \frac{1}{2T}, \tag{16}$$

where T is the integrate-dump time of the FLL.

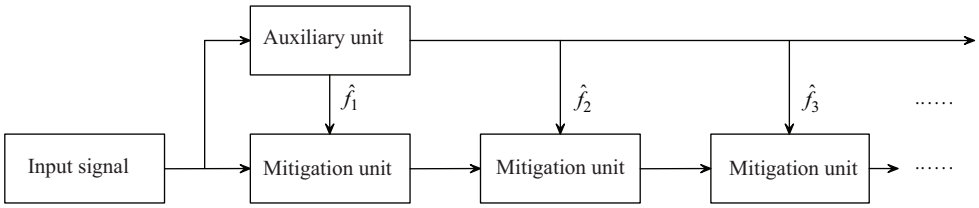

Figure 4 Schematic block diagram of the cascaded mitigation unit.

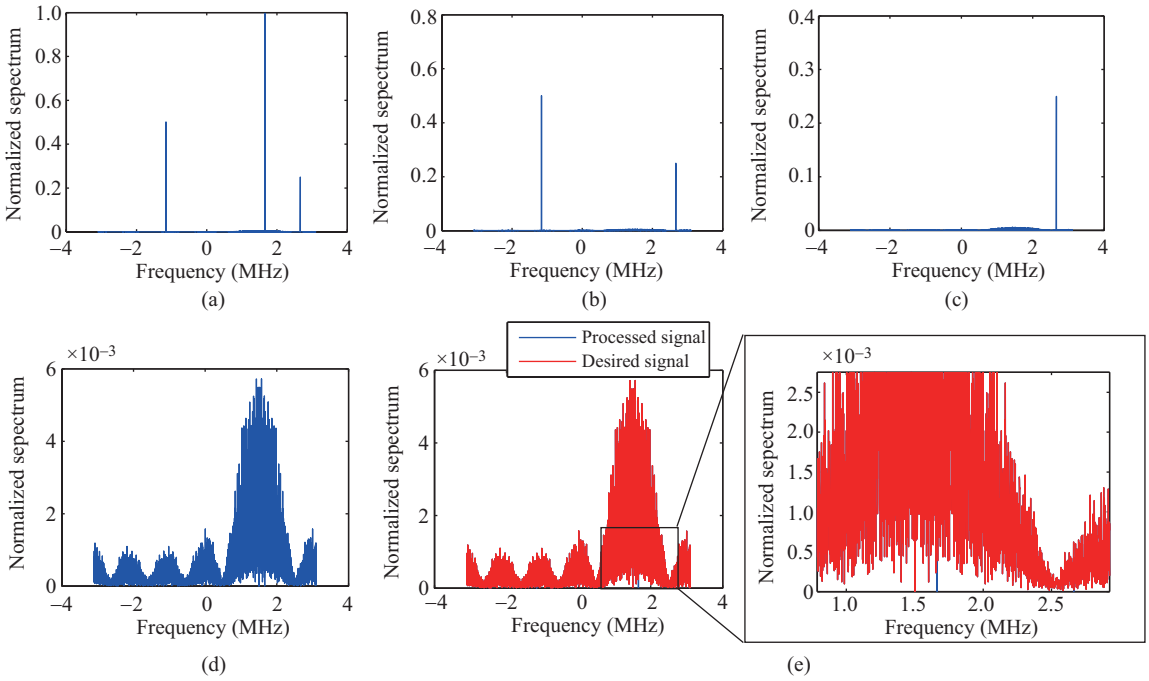

Figure 5 Signal spectrum of the multiple interference mitigation process. (a) Received signal; (b) the strongest interference is eliminated; (c) the second-strongest interference is eliminated; (d) the last interference is eliminated; (e) comparison between processed signal and desired signal.

3.2 Multiple CW interferences

In this section, multiple CW interferences are considered. To mitigate multiple CW interferences, a cascading DFT unit and MUs can be employed. Figure 4 shows the block diagram of the cascaded MU scheme. The first MU in the chain mitigates the most powerful disturbing interference. Then, the other units remove the remaining interferers with progressively decreasing power [8, 10]. Auxiliary information from a DFT unit is shared for all MUs.

The process of multiple interference mitigation is presented in Figure 5. Three interferences shown in Figure 5(a) are used to demonstrate the removing process. Figure 5(b) and (c) show that the strongest and second-strongest interferences have been removed after two interference MUs are cascaded. Figure 5(d) illustrates that the spectra of all three interferences have been filtered out by the multiple-interference mitigation algorithm. The remaining signal spectrum is compared with the desired signal spectrum in Figure 5(e). As indicated in Figure 5(e), with respect to the desired signal and the signal processed by the proposed algorithm, it can be clearly observed that the spectrum is the same in both cases. The exception is at the frequency of 1.662 MHz, where the interference coincides with one of the worst lines in the PN code. This can be explained as follows. This useful PN spectrum line is regarded as part of the CW interference by the proposed MU and will be subtracted from the front-end signal by mistake [19]. This indicates the loss of a useful signal in the case of the proposed algorithm. This type of loss also exists in the case of other suppression algorithms.

The performance of the algorithm in the presence of multiple interferences can be analyzed by consid-

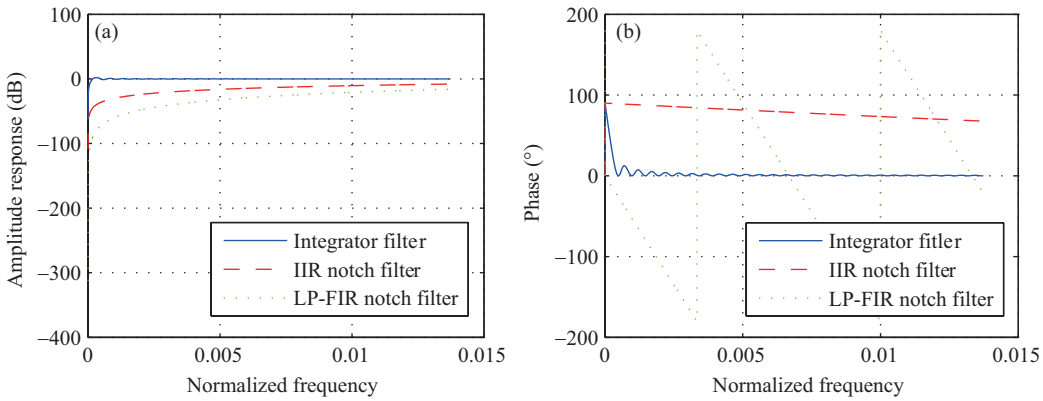

Figure 6 (Color online) Frequency response of interference suppression filter. (a) Amplitude response; (b) phase response.

Table 1 Characteristics of interference suppression filter

Interference suppressor	Normalized bandwidth at −3 dB	Phase response	Implement complexity
Mitigation integrator	8.0204e−04	Approximate to 0	1 multiplier
IIR notch filter	0.0304	Highly non-linear	1 multiplier
LP-FIR notch filter	0.0445	Linear	601 multiplier

ering the single components as independent interfering signals. The multitone signal comprises different waveforms with different characteristics and amplitudes. Naturally, when the analysis is subject to multiple interferences, a similar representation can be established by summing up different contributions.

4 Algorithm performance analysis

4.1 Interference filtering performance

The design of the proposed algorithm can be mainly divided into two parts: interference mitigation and interference adaptive tracking. The interference mitigation process in the proposed algorithm is similar to bandpass filtering. The removal of DC by averaging over integration time T is the same as low-pass filtering with a sinc of bandwidth $1/T$. Thus, the interference suppression performance of the proposed algorithm can be conveniently compared with other time-domain filter methods.

4.1.1 *Interference mitigation*

The interference mitigation process in the proposed algorithm is mainly realized by an integrator. The interference mitigation integrator comprises an accumulator, subtractor, and multiplier; these consume a small amount of hardware resources. The transfer function of the interference mitigation integrator in the proposed algorithm can be given as

$$H(Z) = 1 - \frac{1}{N}\sum_{n=0}^{N-1} Z^{-n} = \frac{N - 1 - Nz^{-1} + z^{-N}}{N\left(1 - z^{-1}\right)}. \tag{17}$$

The frequency response of a digital filter can be interpreted as the transfer function evaluated at $z = \mathrm{e}^{\mathrm{j}w}$. We can write a rational transfer function as

$$H(\mathrm{e}^{\mathrm{j}w}) = \frac{N - 1 - N\mathrm{e}^{-\mathrm{j}w} + \mathrm{e}^{-\mathrm{j}wN}}{N\left(1 - \mathrm{e}^{-\mathrm{j}w}\right)}. \tag{18}$$

Figure 6 depicts the frequency responses of the mitigation integrator, IIR notch filter, and linear phase FIR notch filter. The normalized frequency is set to a range from 0 to 0.08 in order to show the filter characteristics [8,10]. The notch frequency is fixed at 0. The integration time of the integrator is set to 600

sampling points. The bandwidth at −3 dB, the phase response characteristics, and the implementation complexity of the integrator filter, IIR notch filter, and LP-FIR notch filter are summarized in Table 1.

Note that the notch level of the interference mitigation integrator is significantly higher than that of the others, while the notch ability of the 600 order LP-FIR filter is slightly weaker than that of the IIR filter. Thus, it can be concluded that the resource utilization of the mitigation integrator is minimal under the same notch bandwidth conditions. Furthermore, because the LP-FIR notch filter requires a very high order to achieve the same notch depth, the gradient calculation in the LMS adaptive algorithm is considerably complex, which makes the implementation of the interference adaptive process difficult. On the other hand, the phase characteristics of each method are also analyzed. The mitigation integrator and the LP-FIR notch filter are observed to have ideal phase characteristics. The phase of the signal in the pass band remains fairly unchanged after filtering by the integrator filter. The measurement biases introduced by FIR filters can be compensated because of their linear phase property. However, the IIR notch filter has non-linear phase characteristics. The biases in the pseudo range and carrier phase measurements due to the group and the phase delays of the IIR notch filter cannot be easily predicted and compensated.

4.1.2 *Adaptive process*

The adaptive process is based on the FLL used for tracking the interfering signals in the proposed algorithm. Therefore, in this subsection, we analyze its tracking accuracy and then compare it with other adaptive algorithms. The interference adaptive process includes frequency adaption and amplitude adaption. In the proposed algorithm, frequency adaption is realized by the FLL, whereas amplitude estimation is realized by the integrate-dump.

The interference amplitude adaption is an important factor that determines the performance of the interference adaption. In the proposed algorithm, the interference amplitude can be expressed as a mean of the modified integrator output,

$$\hat{A}_i = \frac{1}{N} \times \begin{bmatrix} NA_i \mathrm{sinc}\left(\pi f_e T\right) \mathrm{e}^{\mathrm{i}\left[2\pi f_e\left(t_k+\frac{T}{2}\right)+\theta_e\right]} \\ + \sum\limits_{n=1}^{N} s\left[n-\tau_0\right] \mathrm{e}^{-\mathrm{i}\left(2\pi \hat{f}_i n+\hat{\theta}_i\right)} \\ + \sum\limits_{n=1}^{N} \eta\left[n\right] \mathrm{e}^{-\mathrm{i}\left(2\pi \hat{f}_i n+\hat{\theta}_i\right)} \end{bmatrix} \times \mathrm{e}^{-\mathrm{i}(2\pi f_e n+\theta_e)}. \tag{19}$$

Because the spread spectrum signal is relatively weak, the interference estimation error caused by the spreading signal is ignored. Assuming $s\left[n-\tau_0\right]=0$, we get

$$\hat{A}_i = \begin{bmatrix} A_i \mathrm{sinc}\left(\pi f_e T\right) \mathrm{e}^{\mathrm{i}\left[2\pi f_e\left(t_k+\frac{T}{2}\right)+\theta_e\right]} \\ +\frac{1}{N} \sum\limits_{n=1}^{N} \eta\left[n\right] \mathrm{e}^{-\mathrm{i}\left(2\pi \hat{f}_i n+\hat{\theta}_i\right)} \end{bmatrix} \times \mathrm{e}^{-\mathrm{i}(2\pi f_e n+\theta_e)}. \tag{20}$$

Because interference mitigation is based on FLL tracking, which provides accurate interference synchronization, the interference estimation error caused by the tracking deviation is ignored. Substituting $f_e \approx 0$ into (20), we obtain

$$\hat{A}_i = A_i + \frac{1}{N} \mathrm{e}^{\mathrm{i}\theta_e} \sum_{n=1}^{N} \eta\left[n\right] \mathrm{e}^{\mathrm{i}\left(2\pi \hat{f}_i n+\hat{\theta}_i\right)}. \tag{21}$$

Thus, we have the normalized amplitude estimation as

$$\hat{A}_{i,\mathrm{normalized}} = \frac{\hat{A}_i}{A_i} = 1 + \frac{1}{NA_i} \mathrm{e}^{-\mathrm{i}\theta_e} \sum_{n=1}^{N} \eta\left[n\right] \mathrm{e}^{-\mathrm{i}\left(2\pi \hat{f}_i n+\hat{\theta}_i\right)}. \tag{22}$$

Then, the root-mean-square error (RMSE) of the steady state normalized amplitude $\hat{A}_{i,\mathrm{normalized}}$ can be obtained as

$$\mathrm{rmse}\left(\hat{A}_{i,\mathrm{normalized}}\right) = \left\| \frac{1}{NA_i} \mathrm{e}^{\mathrm{i}\theta_e} \sum_{n=1}^{N} \eta\left[n\right] \mathrm{e}^{-\mathrm{i}\left(2\pi \hat{f}_i n+\hat{\theta}_i\right)} \right\|_2, \tag{23}$$

where $\eta[n]$ is a complex random variable whose real and imaginary parts are zero mean Gaussian random variables. Here, the variance of $\eta[n]$ is given by

$$\mathrm{var}(\eta[n]) = E|\eta[n]|^2 = \sigma^2, \tag{24}$$

where $\sigma^2 = {A_i}^2/\mathrm{JNR}$. Therefore, the variance of the integrate-dump result for the noise term can be derived as

$$\mathrm{var}\left(\sum_{n=1}^{n} \eta[n]\, \mathrm{e}^{-\mathrm{i}\left(2\pi\hat{f}_i n+\hat{\theta}_i\right)}\right) = N\sigma^2. \tag{25}$$

Substituting (25) into (23), the RMSE of the steady state normalized amplitude becomes

$$\mathrm{rmse}\left(\hat{A}_{i,\mathrm{normalized}}\right) = 1/(\sqrt{N \times \mathrm{JNR}}). \tag{26}$$

On the other hand, interference frequency tracking is also an important indicator for the adaptive process. Rule-of-thumb thresholds can be used along with equations that predict the measurement errors of the tracking loops [15]. The rule-of-thumb tracking threshold for the FLL is that the 3-sigma value of the frequency jitter due to all sources of loop stress must not exceed 90° in one predetection integration time, T, or $90/360T$ Hz. Thus, the rule-of-thumb FLL threshold analysis is given by

$$3\sigma_{\mathrm{FLL}} = 3\sigma_{t,\mathrm{FLL}} + f_{e,\mathrm{FLL}} \leqslant \frac{1}{4T}, \tag{27}$$

where $\sigma_{t,\mathrm{FLL}}$ is 1-sigma thermal noise frequency jitter. $f_{e,\mathrm{FLL}}$ is 3-sigma dynamic stress error. T is predetection integration time. A formula for estimating the variance of the thermal noise frequency jitter can be expressed as

$$\sigma_{t,\mathrm{FLL}} = \frac{1}{2\pi T}\sqrt{\frac{4FB_L}{\mathrm{CNR}}\left(1+\frac{1}{T\cdot\mathrm{CNR}}\right)}, \tag{28}$$

where F equals 1 at high CNR, or equals 2 when near threshold. B_n is the FLL loop noise bandwidth. CNR is the carrier-to-noise power ratio.

Figure 7 reports an example of the interference tracking process under several jamming signal-to-noise power ratio (JNR) conditions. The process is compared with the LMS adaptive process of the IIR notch filter [8,10]. The simulation results closely follow the analytical results. The amplitude estimation RMSE in the case of the proposed algorithm is worse than that in the case of the LMS algorithm adaption process under the high JNR condition, while the frequency tracking accuracy of the FLL algorithm is considerably better than that of the LMS algorithm of the IIR notch filter. In addition, the tracking mitigation ability of the weak interference is useful in high-precision ranging and velocity measurements. It is concluded that, in the simulation, the convergence of the LMS algorithm is not good when the signal JNR is lower than −5 dB, while the FLL track threshold can be as low as −20 dB.

4.2 Interference estimation precision

In this section, in order to analyze the overall performance of the interference suppression algorithm, the interference estimation performance of the proposed mitigation algorithm is investigated. Two different metrics, ε_n and ε in [5] are introduced to quantify the effectiveness of the interference mitigation algorithm. Statistic metrics ε_n and ε measure the difference between the estimated interference and the actual interference that represents the interference estimation precision of the interference mitigation algorithm.

Metric ε_n is defined as

$$\varepsilon_n = \left\| \frac{j-\hat{j}}{\|j\|} \right\|^2, \tag{29}$$

and metric ε is defined as

$$\varepsilon = \left\| j-\hat{j} \right\|^2, \tag{30}$$

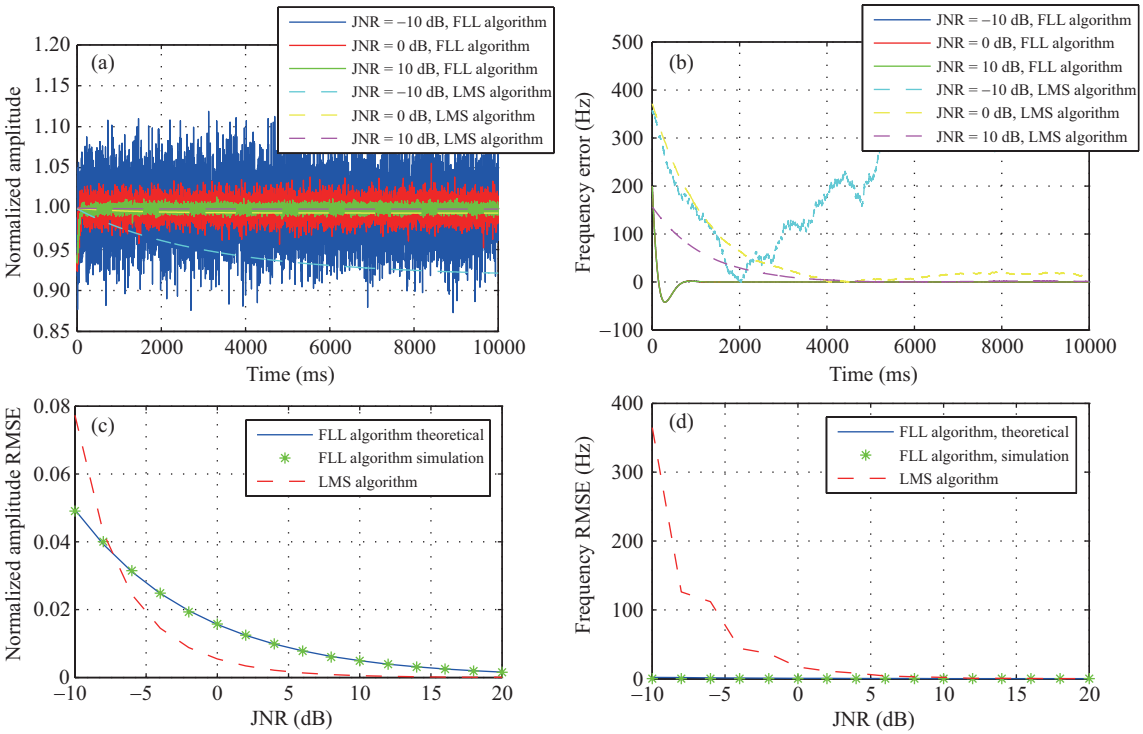

Figure 7 Adaptive process of interference mitigation algorithms.

where j is the actual interference, $\hat{j}$ is the estimated interference, and ε_n can assume the following values:

$$\begin{cases} \varepsilon_n = 0, & \text{in the case of an ideal estimate;} \\ 0 < \varepsilon_n < 1, & \text{in the case of a correct estimate;} \\ \varepsilon_n \geqslant 1, & \text{in the case of a misleading estimate.} \end{cases} \tag{31}$$

When $\varepsilon_n \geqslant 1$, this case is considered to be one where the interference mitigation algorithm is invalid.

Now, we study the performance of the proposed algorithm with the two metrics. According to (13), the estimated interference can be expressed as

$$\hat{j}[n] = \begin{bmatrix} \left\{ A_i \mathrm{sinc}(\pi f_e T) \, \mathrm{e}^{\mathrm{i}\left[2\pi f_e\left(t_k + \frac{T}{2}\right) + \theta_e\right]} \right\} \mathrm{e}^{\mathrm{i}\left(2\pi \hat{f}_i n + \hat{\theta}_i\right)} \\ + \frac{1}{N} \mathrm{e}^{\mathrm{i}\left(2\pi \hat{f}_i n + \hat{\theta}_i\right)} \sum_{n=1}^{N} s[n - \tau_0] \, \mathrm{e}^{-\mathrm{i}\left(2\pi \hat{f}_i n + \hat{\theta}_i\right)} \\ + \frac{1}{N} \mathrm{e}^{\mathrm{i}\left(2\pi \hat{f}_i n + \hat{\theta}_i\right)} \sum_{n=1}^{N} \eta[n] \, \mathrm{e}^{-\mathrm{i}\left(2\pi \hat{f}_i n + \hat{\theta}_i\right)} \end{bmatrix}. \tag{32}$$

In addition, considering the interference model in (3), a single actual interference is declared as

$$j[n] = A_i \mathrm{e}^{\mathrm{i}(2\pi f_i n + \theta_i)}. \tag{33}$$

Accordingly, by substituting (32) and (33) into (30), the expression of metric ε can be derived as

$$\begin{aligned} \varepsilon &= \left\| j - \hat{j} \right\|^2 \\ &= \left\| A_i \mathrm{e}^{\mathrm{i}(2\pi f_i n + \theta_i)} - A_i \mathrm{e}^{\mathrm{i}\left(2\pi \hat{f}_i n + \hat{\theta}_i\right)} \left\{ \begin{array}{l} \mathrm{sinc}(\pi f_e T) \, \mathrm{e}^{\mathrm{i}\left[2\pi f_e\left(t_k + \frac{T}{2}\right) + \theta_e\right]} \\ + \frac{1}{A_i N} \sum_{n=1}^{N} s[n - \tau_0] \, \mathrm{e}^{-\mathrm{i}\left(2\pi \hat{f}_i n + \hat{\theta}_i\right)} \\ + \frac{1}{A_i N} \sum_{n=1}^{N} \eta[n] \, \mathrm{e}^{-\mathrm{i}\left(2\pi \hat{f}_i n + \hat{\theta}_i\right)} \end{array} \right\} \right\|^2. \end{aligned} \tag{34}$$

Table 2 Simulation parameters

Parameter	Symbol	Value
GPS C/A PRN number	PRN	1
Sampling frequency	f_s	4.092 MHz
Coherent integration time	T	0.1 ms, 1 ms, 10 ms
Intermediate frequency	f_0	1.023 MHz
C/N_0	CNR	43 dB/Hz
FLL bandwidth	B_n	4 Hz

In (34), it can be noted that the error term originates from the frequency tracking error f_e, the useful signal $s[n-\tau_0]$, and the noise $\eta[n]$. It is concluded that the interference estimation performance of the proposed algorithm is essentially thermal noise performance. Assuming $s[n-\tau_0]=0$ and $f_e=0$, the statistical metric ε becomes

$$\varepsilon = \left\| \frac{1}{N} \mathrm{e}^{\mathrm{i}\left(2\pi \hat{f}_i n + \hat{\theta}_i\right)} \sum_{n=1}^{N} \eta[n]\, \mathrm{e}^{-\mathrm{i}\left(2\pi \hat{f}_i n + \hat{\theta}_i\right)} \right\|^2. \tag{35}$$

Hence, only the noise in the error term should be mainly considered. Then, according to (25), we obtain

$$\left\| \mathrm{e}^{\mathrm{i}\left(2\pi \hat{f}_i n + \hat{\theta}_i\right)} \sum_{n=1}^{N} \eta[n]\, \mathrm{e}^{-\mathrm{i}\left(2\pi \hat{f}_i n + \hat{\theta}_i\right)} \right\|^2 = N\sigma^2. \tag{36}$$

Thus, the statistical metrics ε_n and ε are obtained as

$$\varepsilon_n \approx \left\| \frac{\sigma^2/N}{\left\| A_i \mathrm{e}^{\mathrm{i}(2\pi f_i n + \theta_i)} \right\|} \right\|^2 = \frac{1}{N \times \mathrm{JNR}}, \tag{37}$$

$$\varepsilon \approx \frac{N\sigma^2}{N^2} = \frac{\sigma^2}{N}. \tag{38}$$

Metrics ε_n and ε respectively denote the relative and absolute values of the interference estimation error obtained with the proposed method. It can be understood that ε_n is correlated with the signal JNR and the sampling number N within the time of integration, while ε is related to noise power and is independent of the power of the interference. The above analytical techniques require much less computational time and effort than simulation techniques employed to predict interference mitigation performance.

5 Simulation results

In this section, simulation results are presented to illustrate the final performance of the proposed mitigation method. Two sets of simulations are presented to verify the effectiveness of the proposed mitigation algorithm. The first set of simulations demonstrates the theoretical analysis of the interference estimation error for the proposed algorithm with the metrics described in Section 4. In addition, the second set of designed simulations shows the applicative performance in terms of the range measurement for the proposed algorithm [20]. This is because the basic function of a GNSS receiver is to determine its location, which can be obtained by estimating the received signal's time of arrival [21].

The scenario adopted for the simulation is characterized by the parameters listed in Table 2. In particular, interference signals with constant amplitude and fixed frequency are presumed in the simulation. The performance of the proposed MU is compared with that of the IIR notch filters, phase-compensated LP-FIR notch filters, DFT N-sigma transform domain algorithm, and interference-free scenario. The parameters of interference mitigation algorithms listed in Table 3 are used in the simulation [8, 10, 13].

Table 3 Parameters of interference mitigation algorithm

Mitigation algorithm	Parameter	Value
Proposed algorithm	Integration time T	$T = 1$ ms
IIR notch filter	z_0, k_a	$z_0 = \exp\{\mathrm{j}2\pi f_i\}$, $k_a = 0.9$
LP-FIR notch filter	z_0, k_a, order	$z_0 = \exp\{\mathrm{j}2\pi f_i\}$, $k_a = 0.9$, $N = 600$ order, and phase-compensated by $N/2f_s$
DFT transform N-sigma algorithm	FFT point N_p	$N_p = 1024$

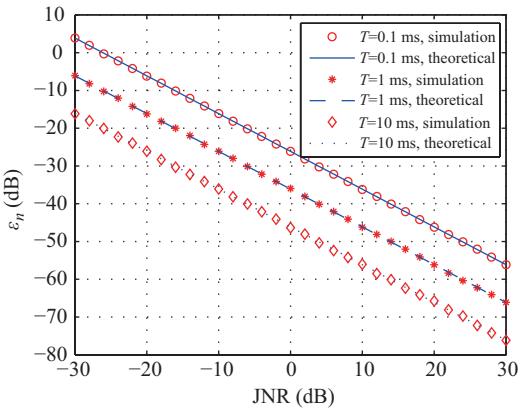

Figure 8 (Color online) Interference estimation precision. ε_n vs JNR.

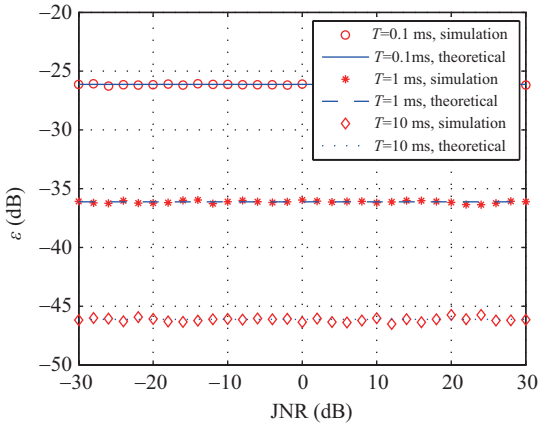

Figure 9 (Color online) Interference estimation precision. ε vs JNR.

5.1 Interference estimation precision

First, the proposed algorithm is simulated in terms of metrics ε_n and ε. The integration time of the FLL is configured as 0.1 ms, 1 ms, and 10 ms, respectively. The performance of the proposed algorithm with regard to the integration time of 1 ms is compared with the performances of the other interference mitigation algorithms. Owing to the large amount of computation of the LP-FIR filter adaptive process, the proposed algorithm cuts off the adaptive module in both notch filter algorithms for simplifying the operation, and the notch filter zero of the two notch filter algorithms is fixed on interference frequency directly. The simulation results are expressed in decibels (dB) to highlight the better performance.

Figures 8 and 9 depict metrics ε_n and ε for the theoretical performance and simulation results under three integration time cases. The simulation results for both metrics agree very well with the theoretical estimation, and verify the accuracy of the analytical expressions. The residual interference power has a small value, and it depends only on noise power; this is evident from (38). Figures 10 and 11 compare the metrics ε_n and ε for the proposed algorithm ($T = 1$ ms) and the other interference mitigation algorithms. As shown in the figure, the DFT algorithm has the worst performance in the simulation because of spectral leakage. The interference mitigation ability of phase-compensated LP-filter is approximately 2 dB better than that of the IIR filter because of better phase characteristics, whereas the proposed algorithm provides a significant improvement of approximately 22 dB over the notch filter algorithms. It is indicated that not only is the interference adaption process of FLL efficient, but the frequency response of the interference mitigation integrator is also ideal.

The results for the analysis and simulation reveal that the interference mitigation algorithm based on the FLL is efficient in interference estimation. When compared to the other mitigation algorithms, the estimated interference in the proposed algorithm is exactly identical to the real interference, and the residual interference power has a constant low value in each JNR case. The performance of the proposed algorithm can be adjusted by modifying the parameter integration time T. Reducing the integration time T can increase the interference dynamic adaptation range. Further, a longer T increases the interference mitigation ability.

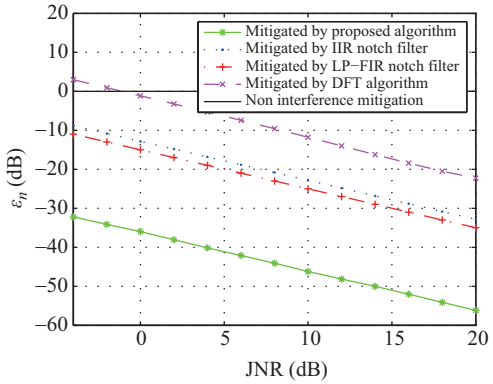

Figure 10 (Color online) Mitigation algorithms. ε_n vs JNR.

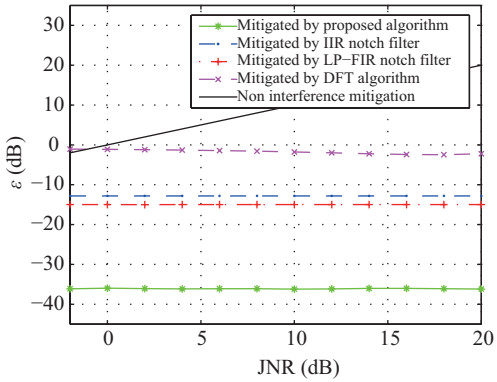

Figure 11 (Color online) Mitigation algorithms. ε vs JNR.

Table 4 RMSE of the code tracking error (m)

JNR	Proposed algorithm	DFT algorithm	Adaptive IIR filter	Adaptive LP-FIR filter	Non-mitigation
10 dB	0.1882	1.4352	3.2567	0.2872	3.1657
4 dB	0.1538	0.5136	3.1397	0.2556	2.1908
0 dB	0.1101	0.2681	3.1395	0.3022	1.7501
−4 dB	0.1356	0.1422	2.9566	0.3777	1.3591
−10 dB	0.1293	0.0894	2.2658	0.2590	0.8073
Non-interference	0.1714	0.0934	0.9884	0.1658	0.1117

5.2 Receiver tracking performance

The second set of simulations also considers the parameters listed in Table 2 and simulates the performance of the algorithm for interference signals with five different power levels in terms of interference suppression at the tracking stage. In order to compare the adaptive algorithm performance of the notch filter at the same time, the notch filter adaptive mechanism is added in the simulations. The performance is evaluated by the RMSE of code tracking. An interference with a frequency deviation of 72 kHz relative to the intermediate frequency is simulated. This is because the 72nd line of the code spectrum is the worst case for PRN 31, and a severe code tracking bias follows when the CW interference signal coincides with code spectral lines, according to the literature [22, 23]. In this simulation, the RMSE of code tracking is assessed when the delay-locked loop (DLL) successfully tracks in the steady state condition for 10 s.

Table 4 explicitly compares the quantitative performance enhancement of the proposed interference mitigation algorithm. In the table, in the row of non-interference, the damage to useful signal introduced by interference mitigation algorithms is revealed. Note that the adaptive IIR filter brings a significant bad impact on the signal because of the non-linear phase characteristics. The presence of such filters in GNSS receivers induces amplitude and phase distortions, which can lead to some biases in the pseudo range and carrier phase measurements. In a longitudinal comparison, it can be noted that the N-sigma DFT algorithm has a good performance under the weak interference condition; however, it cannot cope with strong interference because the interference frequency lies between the two lines of FFT, and the spectral leakage under high JNR leads to a sharp deterioration of signal quality. In addition, horizontal comparison is used to show that the code tracking error of the proposed algorithm is approximately half the value of the phase-compensated adaptive LP-FIR algorithm. This is because the LP-FIR filter based on the moving average model does not have strong interference notch ability, and a high number of taps results in considerable resource consumption. Thus, the mitigation strength of the proposed algorithm is demonstrated.

The results show the applicative performance characteristics of the mitigation algorithms. The receiver tracking performance shown in the results indicates that the proposed mitigation algorithm has good

phase characteristics and strong interference mitigation ability with low resource consumption. It is illustrated that the proposed algorithm has excellent performance in the interference environment as in the interference-free case.

6 Conclusion

This paper proposes and presents an analysis of an interference mitigation algorithm based on FLL. The FLL and mitigation integrator bring advantages to the proposed algorithm. The simulation results show that the proposed algorithm with excellent interference estimation precision has superior anti-jamming performance. The interference-tracking FLL and mitigation integrator in the design filtering interference without causing phase distortion. The two metrics related to the interference estimation error demonstrate that the proposed algorithm provides an improvement of 22 dB over the notch filter algorithm. The receiver tracking performance shows that the proposed mitigation algorithm performs well in all of the various JNR cases as well as in the interference-free case and outperforms the other algorithms. This paper focuses on the mitigation of fixed-frequency CW interference. Future work with the proposed algorithm will involve extending the scope to mitigation algorithms under dynamic conditions.

Acknowledgements This work was supported by National High Technology Research and Development Program of China (863) (Grant No. 2013AA1548), and National Natural Science Foundation of China (Grant No. 61401026).

Conflict of interest The authors declare that they have no conflict of interest.

References

1 Kaplan E D, Hegarty C J. Understanding GPS: Principles and Applications. 2nd ed. Norwood: Artech House, 2005. 153–300
2 Chang C L, Juang J C. Performance analysis of narrowband interference mitigation and near-far resistance scheme for GNSS receivers. Sign Proc, 2010, 90: 2676–2685
3 Wang Y Q, Li C, Xu D, et al. A new barycenter code discriminator for multi-access interference. Sci China Inf Sci, 2014, 57: 022311
4 Borio D. GNSS acquisition in the presence of continuous wave interference. IEEE Trans Aero Electron Syst, 2010, 46: 47–60
5 Savasta S, Presti L L, Rao M. Interference mitigation in GNSS receivers by a time-frequency approach. IEEE Trans Aero Electron Syst, 2013, 49: 415–438
6 Balaei A T, Motella B, Dempster A. A preventative approach to mitigating CW interference in GPS receivers. GPS Solutions, 2008, 12: 199–209
7 Borio D, Camoriano L, Savasta S, et al. Time-frequency excision for GNSS applications. IEEE Syst J, 2008, 2: 27–37
8 Lin T, Abdizadeh M, Broumandan A. Interference suppression for high precision navigation using vector-based GNSS software receivers. In: Proceedings of ION GNSS, Portland, 2011. 20–23
9 Punchalard R. Mean square error analysis of unbiased modified plain gradient algorithm for second-order adaptive IIR notch filter. Sign Proc, 2012, 92: 2815–2820
10 Borio D, Camoriano L, Presti L L. Two-pole and multi-pole notch filters: a computationally effective solution for GNSS interference detection and mitigation. IEEE Syst J, 2008, 2: 38–47
11 Petovello M, Borio D, Dovis F, et al. Impact of notch filtering on tracking loops for GNSS applications. Dissertation for Master Degree. Canada: UCalgary, 2009. 19–55
12 Ojeda O A, Grajal J, Lopez R G. Analytical performance of GNSS receivers using interference mitigation techniques. IEEE Trans Aero Electron Syst, 2013, 49: 885–906
13 Capozza P T, Holland B J, Hopkinson T M, et al. A single-chip narrow-band frequency-domain excisor for a global positioning system (GPS) receiver. IEEE J Solid-State Circ, 2000, 35: 401–411
14 Balaei A T, Dempster A G. A statistical inference technique for GPS interference detection. IEEE Trans Aero Electron Syst, 2009, 45: 1499–1511
15 Ward P W. Performance comparisons between FLL, PLL and a novel FLL-assisted-PLL carrier tracking loop under RF interference conditions. In: Proceedings of the 11th International Technical Meeting of the Satellite Division of the Institute of Navigation (ION GPS 1998), Nashville, 1998. 783–795
16 Foucras M, Ekambi B, Ngayap U, et al. Performance study of FLL schemes for a successful acquisition-to-tracking transition. In: Proceedings of IEEE/ION Position, Location and Navigation Symposium—PLANS, Monterey, 2014.

529–540
17 Quinn B G. Estimating frequency by interpolation using fourier coefficients. IEEE Trans Signal Process, 1994, 42: 1264–1268
18 Provencher S. Parameters estimation of complex multitone signal in the DFT domain. IEEE Trans Signal Process, 2011, 59: 3001–3012
19 Betz J W, Kolodziejski K R. Generalized theory of code tracking with an early-late discriminator part ii: noncoherent processing and numerical results. IEEE Trans Aero Electron Syst, 2009, 45: 1557–1564
20 Balaei A T, Dempster A G, Presti L L. Characterization of the effects of CW and pulse CW interference on the GPS signal quality. IEEE Trans Aero Electron Syst, 2009, 45: 1418–1431
21 Wang Y Q, Gao L, Wu S L. Design of code tracking loop for spacecraft TT&C transponder (in Chinese). J Beijing Univ Posts and Telecommun, 2010, 33: 49–53
22 Liu Y Q, Ran Y H, Ke T, et al. Code tracking performance analysis of GNSS signal in the presence of CW interference. Sign Proc, 2011, 91: 970–987
23 Jang J, Paonni M, Eissfeller B. CW interference effects on tracking performance of GNSS receivers. IEEE Trans Aero Electron Syst, 2012, 48: 243–258